Reinforcing of a Calcium Phosphate Cement with Hydroxyapatite Crystals of Various Morphologies: Biocomposite @BULLET calcium phosphate cement @BULLET reinforcement @BULLET mechanic...

ARTICLE *in* ACS APPLIED MATERIALS & INTERFACES · NOVEMBER 2010

Impact Factor: 6.72 · DOI: 10.1021/am100710b

6 AUTHORS, INCLUDING:

Krishna P. Kommareddy
University of Cincinnati
14 PUBLICATIONS **194** CITATIONS
SEE PROFILE

Manjubala Inderchand
VIT University
53 PUBLICATIONS **1,256** CITATIONS
SEE PROFILE

Masahiro Yoshimura
National Cheng Kung University
828 PUBLICATIONS **15,158** CITATIONS
SEE PROFILE

Francisco Guitián
University of Santiago de Compostela
125 PUBLICATIONS **1,791** CITATIONS
SEE PROFILE

ARTICLE

Reinforcing of a Calcium Phosphate Cement with Hydroxyapatite Crystals of Various Morphologies

Inés S. Neira,*,†,‡,§ Yury V. Kolen'ko,‡,∥ Krishna P. Kommareddy,§ Inderchand Manjubala,§ Masahiro Yoshimura,‡ and Francisco Guitián†

Galician Institute of Ceramics, University of Santiago de Compostela, E-15782 Santiago de Compostela, Spain, Materials and Structures Laboratory, Tokyo Institute of Technology, 4259 Nagatsuta, Midori-ku, 226-8503 Yokohama, Japan, Department of Biomaterials, Max Planck Institute of Colloids and Interfaces, D-14424 Potsdam, Germany, Present address: International Iberian Nanotechnology Laboratory, 4710-299 Braga, Portugal

ABSTRACT A series of biocomposite materials was successfully prepared by reinforcing advanced calcium phosphate cement with hydroxyapatite fibrous and elongated plate-like particles. Powder X-ray diffraction showed that ball-milled biocomposite precursors (dicalcium and tetracalcium phosphates) entirely transform to a single phase hydroxyapatite end product within 7 h at 37 °C. Electron microscopy showed that the resultant biocomposites are constituted of nanoscaled cement particles intimately associated with the reinforcement crystals. The influence of shape, size, and concentration of the hydroxyapatite filler on the compression strength of reinforced cements is discussed. The best compression strength of 37 ± 3 MPa (enhancement of ∼50% compared to pure cement) was achieved using submicrometer-sized hydroxyapatite crystals with complementary shapes. Nanoindentation revealed that averaged elastic modulus and hardness values of the cements are consistent with those reported for trabecular and cortical human bones, indicating a good match of the micromechanical properties for their potential use for bone repair. The stiffness of the biocomposites was confirmed to gradate—compliant cement matrix, cement-filler interface, and stiff filler—as a result of the structuring at the nanometer−micrometer level. This architecture is critical in conditioning the final mechanical properties of the functional composite biomaterial. *In vitro* cell culture experiments showed that the developed biomaterial system is noncytotoxic.

KEYWORDS: Biocomposite • calcium phosphate cement • reinforcement • mechanical properties • micromechanical properties • compression strength • nanoindentation • stiff interface

INTRODUCTION

Although fractured bones can repair themselves, there are some situations where natural reparation and reconstruction of the hard tissue are limited or tend to not heal correctly. In such cases, bones may require repair or substitution in the course of a surgical procedure. From the viewpoint of biomaterial and biomedical research, calcium phosphate cements (CPCs) are promising materials that can be effectively used for bone repair and substitution (1, 2). Several reviews covering the preparation, properties, and applications of CPC biomaterials are available (3−7). The current uses of CPCs are broadly related to craniofacial and periodontal applications, while attempts to use cements in the areas where bones support dynamic load (load-bearing applications) have failed to give long-term performance. This is due to the lower fracture toughness parameter of CPCs (∼0.6−1.5 MPa/m^2) (8) in contrast to human bones (∼2−12 MPa/m^2) (9).

One of the most promising strategies to improve the mechanical performance (strength and fracture toughness) of the CPCs is their reinforcement *via* physical linking of spatially allocated fibrous materials (7, 10). The most appealing feature of such biocomposites is that the filler is mechanically stronger than the matrix, and therefore, being thoroughly embedded in the cement, it can prevent potential crack propagation. There are two types of reinforcement phases: bioinert and bioactive. In the case of a bioinert approach, examples include the reinforcement of hydroxyapatite (HA, $Ca_{10}(PO_4)_6(OH)_2$) ceramics by adding various biocompatible fibers, such as polymers (11, 12), C (13), SiC (13), ZrO_2 (14), or Al_2O_3 (15) to improve their mechanical properties. Ordinarily, the bioactivity and bioresorbability of such composites is reduced, as the bioinert fillers do not interact with the host tissue. These limitations have strongly motivated research related to bioactive reinforcements. For instance, the application of HA (16, 17) or β-tricalcium phosphate (18) fibers with excellent biological and physiological characteristics as a reinforcement phase has recently attracted considerable attention. The main advantage of these materials is that all of their components are biocompatible, bioactive, and reasonably osteoconductive.

* Corresponding author. Phone: +34-981563100, ext. 16885. Fax: +34-981564242. E-mail: ines.sanchez@usc.es.

Received for review August 8, 2010 and accepted September 24, 2010

† University of Santiago de Compostela.

‡ Tokyo Institute of Technology.

§ Max Planck Institute of Colloids and Interfaces.

∥ Present address: International Iberian Nanotechnology Laboratory, 4710-299 Braga, Portugal.

DOI: 10.1021/am100710b

Published on Web 11/01/2010

Table 1. Specification, Phase Composition, and Compression Strength of Reinforced Biocomposite Cements

sample	shape, length *L*, and diameter *D* of the HA filler (20)	amount of the HA filler (wt %)	XRD phase composition	compression strength (MPa)[a]
	selection of the optimal particle morphology			
pure CPC[b]			HA	25 ± 3
CPC−10%PT	plate-like; *L*, a few μm to a few tenths of a μm	10	HA	27 ± 1[c]
CPC−10%ND	needle-like; *L*, several tenths of a μm to a few hundredths of a μm	10	HA	28 ± 2[c]
CPC−10%HX	hexagonal prism-like; *L*, a few tenths of a μm; *D*, ~2 μm	10	HA	30 ± 3
CPC−10%FP	fine-plate-like; *L*, a few hundredths of a nm to a few μm	10	HA	37 ± 3
	selection of the optimal volume fraction			
CPC−5%HX	hexagonal prism-like	5	HA	31 ± 3[d]
CPC−10%HX		10	HA	30 ± 3[e]
CPC−15%HX		15	HA	33 ± 2[f]
CPC−20%HX		20	HA	27 ± 0.6[g]
CPC−30%HX		30	HA	26 ± 4[h]
CPC−5%FP	fine-plate-like	5	HA	31 ± 4[i]
CPC−10%FP		10	HA	37 ± 3
CPC−15%FP		15	HA	29 ± 4[i]
CPC−20%FP		20	HA	23 ± 1[j]
CPC−30%FP		30	HA	20 ± 0.3

[a] CS values statistically significant different ($P < 0.05$, *t* test). [b] Pure CPC is reported calcium phosphate cement C-D36/T48 (19). [c] CPC−10%ND and CPC−10%PT are not statistically different from each other. [d] Not statistically different from CPC−10%HX, CPC−15%HX, CPC−20%HX, and CPC−30%HX. [e] Not statistically different from CPC−5%HX, CPC−20%HX, and CPC−30%HX. [f] Not statistically different from CPC−5%HX. [g] Not statistically different from CPC−5%HX, CPC−10%HX, and CPC−30%HX. [h] Not statistically different from CPC−5%HX, CPC−10%HX, CPC−20%HX, and pure CPC. [i] CPC−5%FP and CPC−15%FP are not statistically different from each other. [j] Not statistically different from pure CPC.

In spite of the great interest in bioactive reinforcement by HA fibrous particles (16, 17), systematic studies of the effect of the shape, size, and concentration of crystals on the mechanical function of the biocomposites have rarely been conducted. In our previous investigations, we successfully synthesized bioactive and noncytotoxic CPCs exhibiting rapid conversion to HA (19) as well as HA crystals with various well-defined particle shapes (plate-like, hexagonal prism-like, needle-like, and fine-plate-like) and sizes (20). In this study, we coupled these matrix and filler materials with the aim of exploring a new family of reinforced biocomposite cements. Marked improvement and sophisticated control over mechanical properties of engineered biocomposites were achieved by varying either the shape and dimension or concentration of the HA filler. The micromechanical properties of such biocomposite CPCs are largely unknown and are studied here by means of nanoindentation.

EXPERIMENTAL SECTION

Biocomposite Preparation. Hydroxyapatite CPC was produced from reactive submicrometer-sized dicalcium phosphate dihydrate (DCPD, $CaHPO_4 \cdot 2H_2O$) and tetracalcium phosphate (TTCP, $Ca_4(PO_4)_2O$) *via* a dissolution−precipitation reaction using water as the liquid phase (21). In a typical procedure, equimolar amounts of ball-milled DCPD and TTCP powders with average particle sizes of approximately 1.1 and 1.5 μm, respectively (19), were thoroughly mixed with the desired amount (Table 1) of HA filler with a plate-like, hexagonal prism-like, needle-like, or fine-plate-like particle morphology generated by a urea-assisted hydrothermal method (Figure 1) (20). The fine powder mixture (0.6 g) was placed inside a latex finger cot, along with an appropriate amount of distilled water, and then hand kneaded for 1 min. The used solid to liquid ratio was 3 g/mL, wherein HA filler was not considered. The resulting putty-like material was then subjected to setting (*vide infra*).

Throughout this work, a set of acronyms are used (Table 1). The first three letters CPC indicate the calcium phosphate cement matrix, the numbers show weight percentages (wt %) of the respective reinforcement phase, while the last two letters reflect the particle morphology of the filler: PT, plate-like; HX, hexagonal prism-like; ND, needle-like; FP, fine-plate-like.

Biocomposite Characterization. Powder X-ray diffraction (XRD) patterns of the biocomposites were collected on a Rigaku RINT 2000 diffractometer, equipped with Ni-filtered Cu Kα radiation ($\lambda = 1.54178$ Å). All diffractograms were collected with a scan speed of 0.5° 2θ/min, and a 0.02° step width. The morphology of the biocomposite CPC was observed by scanning electron microscopy (SEM) using a Hitachi S-4500 microscope, operating at 15 kV. The fine microstructure of the biomaterials was studied by transmission electron microscopy (TEM) and high-resolution TEM (HRTEM) on a Hitachi H-8100 microscope, operating at 200 kV. The samples for TEM were crushed, dispersed in ethanol, and deposited on a holey carbon grid.

Setting of Cement. For HA conversion studies, the aforementioned putty-like paste was rapidly shaped into a rod, divided into several pieces, and allowed to set for 1 h under ambient conditions. Each piece was separately incubated in distilled water at 37 °C for a specific period of time. Immediately prior to the XRD analysis, the test sample was very quickly ground in warm acetone using a hot agate mortar and pestle (80 °C), in order to remove the rest of the water and, to some extent, suspend the reaction process.

For the mechanical property measurements, the biocomposite specimens were prepared by pressing the putty-like material under 5.3 MPa (lowest pressure of the loading device) for 1 min. The obtained biocomposite cylindrical specimens with an aspect ratio of 2 (diameter, 6.9 mm; length, 13.8 mm) were kept for 1 h under ambient conditions to set, incubated in distilled water at 37 °C for 23 h, and then subjected to the mechanical tests.

For *in vitro* tests, 3 times less putty-like biocomposite paste was used. The specimens, in the form of pellets, were prepared by pressing under 5.3 MPa for 1 min. The sample was removed

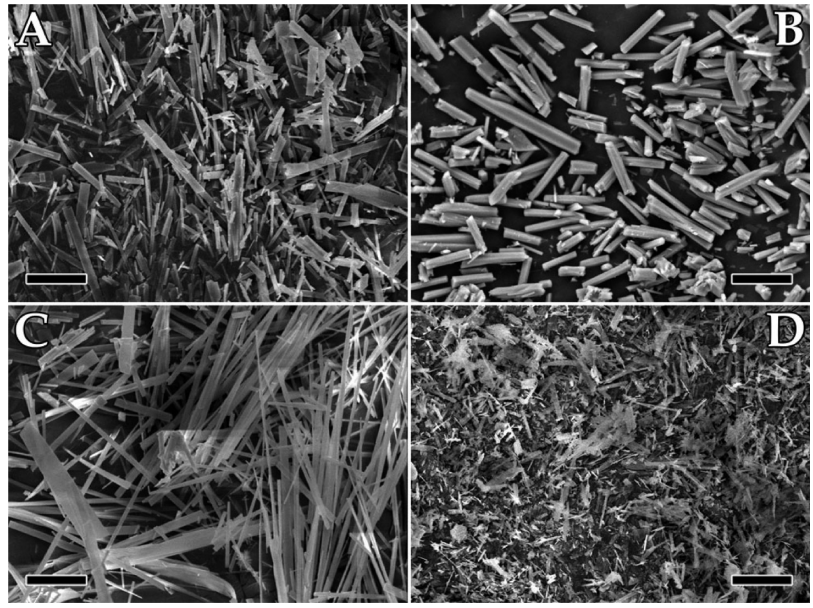

FIGURE 1. SEM images (scale bar 15 μm) of HA reinforcement phases with different shapes: plates (A), hexagonal prisms (B), needles (C), and fine plates (D).

from the mold and kept for 1 h under ambient conditions to set prior to *in vitro* testing.

Mechanical Tests. Compression strength (CS) tests were performed using a Shimadzu Autograph AG-I universal testing machine. All CS values are the average of at least six replicates. Micromechanical properties of the produced cements (elastic modulus E_s and hardness H) were measured using nanoindentation (NI). For this purpose, specimens were embedded in poly(methyl methacrylate), cut with a diamond circular saw, ground with silicon carbide sandpapers, and thoroughly polished with diamond paste down to a particle size of 1 μm. Quasi-static NI on a polished cross-section of the specimens was performed using a Hysitron TriboScan UBI-1 nanohardness tester in conjunction with a Digital Instruments Nanoscope III atomic force microscope (AFM). A Berkovich diamond indenter tip with a nominal radius of 300 nm was used. The system calibration, drift correction (thermal and during unloading), and calculation of the reduced modulus E_r and H from the load−displacement curve were carried out using the software program implemented in the TriboScan, which employs the Oliver and Pharr method (22). Reduced modulus E_r is related to elastic modulus E_s through the following equation: $1/E_r = (1 - \nu_i^2)/E_i + (1 - \nu_s^2)/E_s$, where $\nu_i = 0.07$ is the Poisson's ratio for the diamond tip (23), $\nu_s = 0.28$ has been chosen as the Poisson's ratio for synthetic HA (24), and $E_i = 1141$ GPa is the elastic modulus of the diamond (23). The following loading function was employed: a loading rate of 0.2 mN/s to a peak load of 1 mN, a holding time of 60 s, an unloading to 0.1 mN with a rate of 0.2 mN/s, holding for 20 s, and finally unloaded completely with a rate of 0.5 mN/s. Arrays of indents 13 × 13 with a distance between single indents of 2.5 μm were conducted to create moduli maps.

In Vitro Test. Cytocompatibility of the prepared biomaterials was studied *in vitro* through cell culture experiments, adopted from that of Manjubala et al. (25), using murine preosteoblastic cells (MC3T3-E1) from mouse calvarie. Usually, 5×10^5 cells were suspended in 100 μL of culture medium and seeded on the biocomposite specimens. The specimens were kept at 37 °C for 30 min in Petri dishes to allow the cells to adhere to the surface, and then 2 mL of the medium was added. The medium and Petri dish were refreshed twice a week. To probe differentiation and viability of MC3T3-E1 cells, ALP (alkaline phosphatase) and MTT (3-(4,5-dimethylthiazol-2-yl)-2,5-diphenyltetrazolium bromide) enzyme activity assays were performed. Time points of measurements were on days 8, 14, and 21 for the ALP assay and on days 1, 2, 4, 7, 14, and 21 for the MTT assay. The efficiency of the cell proliferation and distribution over the biocomposite surface were analyzed using a light microscope employing the Giemsa staining histological method. All enzyme activity assay experiments were reproduced in duplicate.

RESULTS

The CPC setting reaction is a result of the dissolution and precipitation processes. Upon mixing with the liquid phase at ambient temperature, the DCPD and TTCP precursors are dissolved, and accordingly, the liquid phase is saturated with phosphate and calcium ions. Then, the nucleation and growth of crystals of a less-soluble calcium phosphate compound, *viz*. Ca-deficient HA, takes place. During precipitation, the HA crystals interlock, thus generating the structural solidity of the cement. The summary of the specification, phase composition, and compression strength of all prepared reinforced biocomposite cements is presented in Table 1. Powder XRD analysis shows that all reinforced biocomposites after 1 h of setting at ambient conditions and subsequent incubation in water for 23 h are phase-pure hexagonal hydroxyapatite (Table 1, Figure 2A). The XRD patterns are characterized by low intensities and very broad peaks; this is a result of the nanocrystalline nature and defective HA structure of the pure cement matrix (19).

To study the influence of the presence of the highly crystalline HA filler on the biocomposite cements setting, the conversion to the HA end product was investigated using XRD. It was established that all biocomposites entirely convert to the HA end product after 7 h of the setting reaction (e.g., CPC−10%FP, Figure 2B). More specifically, according to XRD, CPC−10%FP at $t = 0$ consists of, as expected, DCPD, TTCP, and HA. Further phase analysis reveals total consumption of DCPD already at $t = 5$ h, while TTCP is fully exhausted at $t = 7$ h. The powder XRD patterns of this biocomposite at $t = 7$, 8, and 24 h are very much

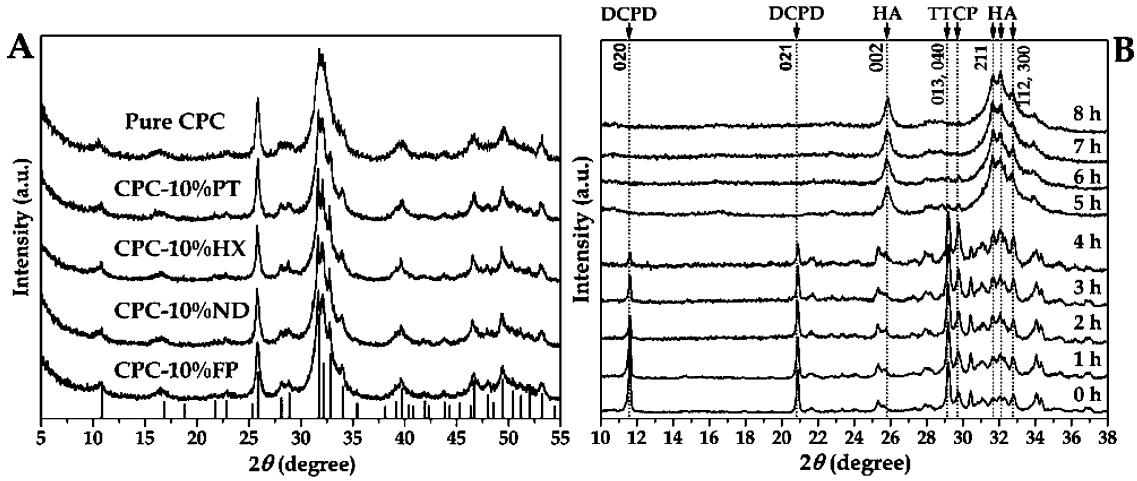

FIGURE 2. (A) Powder XRD patterns of the reinforced cements and pure CPC products after setting for 1 h at ambient conditions and consequent incubation in distilled water at 37 °C for 23 h. Tick marks below the patterns correspond to the positions of the Bragg reflections expected for the hexagonal hydroxyapatite phase (ICDD no. 72−1243). (B) Comparison of the powder XRD patterns at different times of the CPC-10%FP biocomposite setting. The dotted lines correspond to the most intense diffraction peaks of the DCPD and TTCP cement precursors and HA product (ICDD no. 9−77, 70−1379, and 72−1243, respectively).

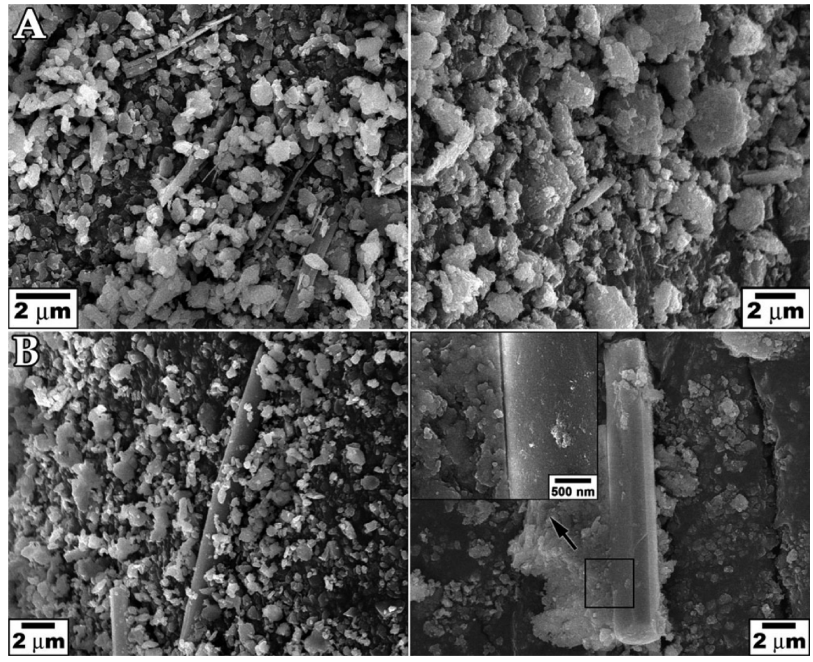

FIGURE 3. SEM images of the CPC−10%FP (A) and CPC−15%HX (B) biocomposites directly after fine mixing of the DCPD and TTCP cement precursors with HA filler (left panels) and after 24 h of their setting (right panels). The inset in B is the respective high magnification SEM.

similar, and no distinction in phase composition, patterns, shapes, and positions/intensities of Bragg reflections of an apatite phase are detected (Figure 2). This indicates that the conversion rate of the biocomposite to HA appears to be very high, and the dissolution−precipitation reaction is fully complete after 7 h of cement setting. Interestingly, the pure cement converts to HA within 6 h (19). This result suggests that the presence of the crystalline HA reinforcement phase does not lead to remarkable changes in the cement matrix setting. The observed 1 h difference appears to result from the lesser amount of water employed in the course of the reinforced biocomposite preparation.

The morphology and nanostructure of the biocomposites were investigated using SEM and TEM (Figures 3 and 4), which confirm a pronounced physical interplay between the cement matrix and reinforcement phase crystals, comprehensively generating an associated microstructure of the end biocomposites. After CPC setting, the interlocked nanoscaled platelet cement crystals are well adhered to the surface of the filler HA crystals. Electron microscopy also demonstrates uniform spatial distribution of the filler particles throughout the biocomposite, with no evidence of intergrowth between the cement nanocrystallites and the reinforcement phase.

Pure cement has a compression strength of 25 ± 3 MPa (mean ± standard deviation) (19). To enhance its mechanical performance as a whole and to improve the CS in particular, this CPC was reinforced with HA crystals with different morphologies. Four biocomposites were generated using the same content of the filler (10 wt %) to select the optimal particle morphology(s) with respect to an increase

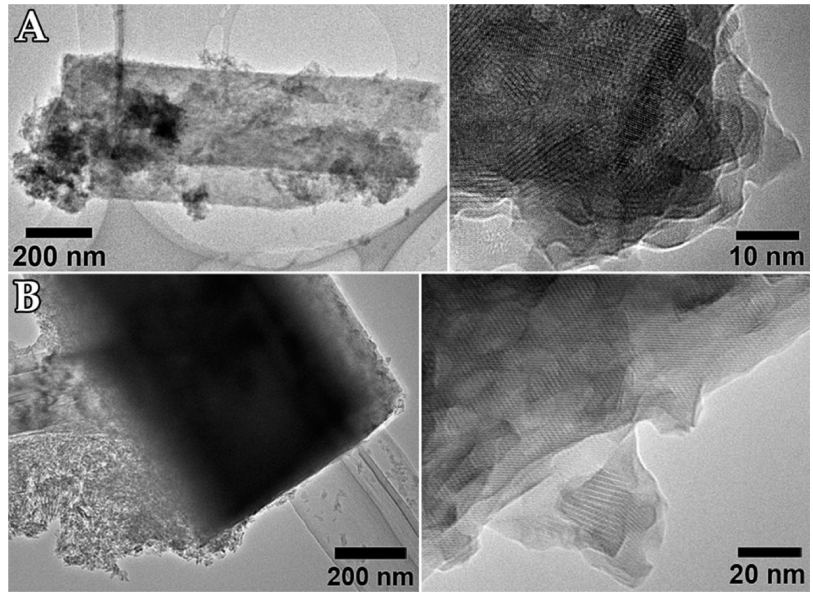

FIGURE 4. Low-magnification (left panels) and high-resolution (right panels) TEM images of the CPC−10%FP (A) and CPC−15%HX (B) biocomposites.

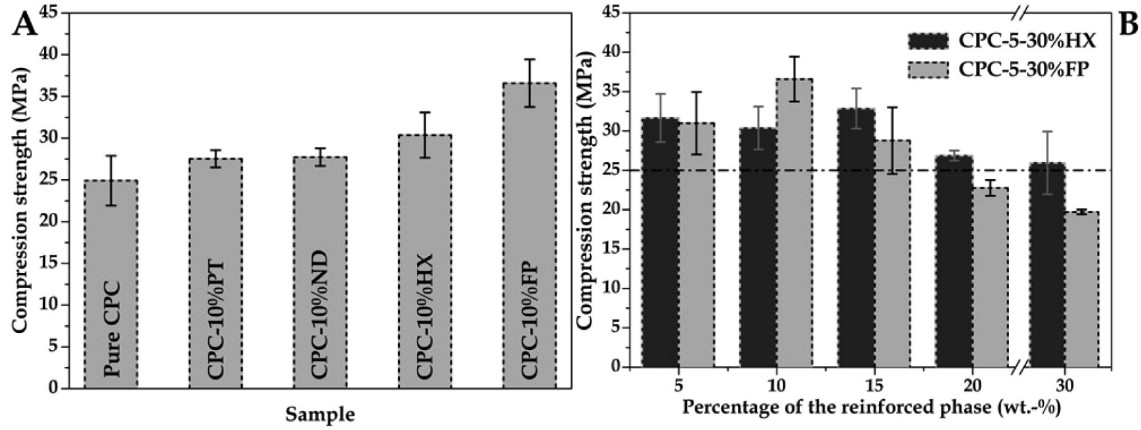

FIGURE 5. Bar graphs of the compression strength performance of the biocomposites as a function of HA filler morphology (A) and concentration (B). The black dashed line in B represents the CS value obtained for pure cement (25 ± 3 MPa) (19).

in the compression strength. Table 1 together with Figure 5A compares the compression strength for the four as-prepared biocomposites. All reinforced cements exhibit enhanced CS. In particular, the biocomposites with hexagonal prism- and fine-plate-like particle morphologies as filler show statistically different and considerably increased compression strength compared to that of pure CPC (up to ∼20 and ∼50%, respectively), while reinforcement with plates and needles (statistically not significantly different) results in a moderate increase of CS by ∼12% (Figure 5A). A maximum value of 37 ± 3 MPa for the CPC−10%FP biocomposite is achieved.

Furthermore, the most effective geometries' appearances (fine-plates and hexagonal prisms) for the stiffening of the cement have been chosen to investigate the effects of filler amount on the mechanical response of the resultant biocomposites. A series of reinforced CPCs with the respective HA particles having a filler content of 5, 10, 15, 20, or 30 wt % was generated (Table 1). In Figure 5B, the resulting CS values as a function of the amount of added filler are compared. Upon reinforcement, the compression strength first increases, reaching a maximum of ∼33 and ∼37 MPa at 15 wt % hexagonal prisms (CPC−15%HX) and 10 wt % fine-plates (CPC−10%FP), respectively. At higher weight loadings, CS values of biocomposites are not statistically different from the value found for pure, unreinforced cement (CPC-30%HX and CPC-20%FP), stay close to this value (CPC-20%HX), or decrease to values lower than that of pure CPC for CPC-30%FP (Table 1, Figure 5B).

The micromechanical properties of pure CPC and one of the strongest biocomposites, CPC-15%HX, were further evaluated and compared by nanoindentation. Arrays of indents with a distance between indents of 2.5 μm were performed. In order to differentiate between the responses to mechanical load of the filler and cement matrix, it was required to use a peak load not higher than 1 mN; otherwise, the size of indentation became larger than the width of the hexagonal shaped HA filler (>2 μm).

The key results from this NI study are shown in Figure 6. The AFM image displayed in Figure 6A was acquired after probing of the pure cement. The resultant array of indents is well-ordered, and the indent impressions are quite narrow

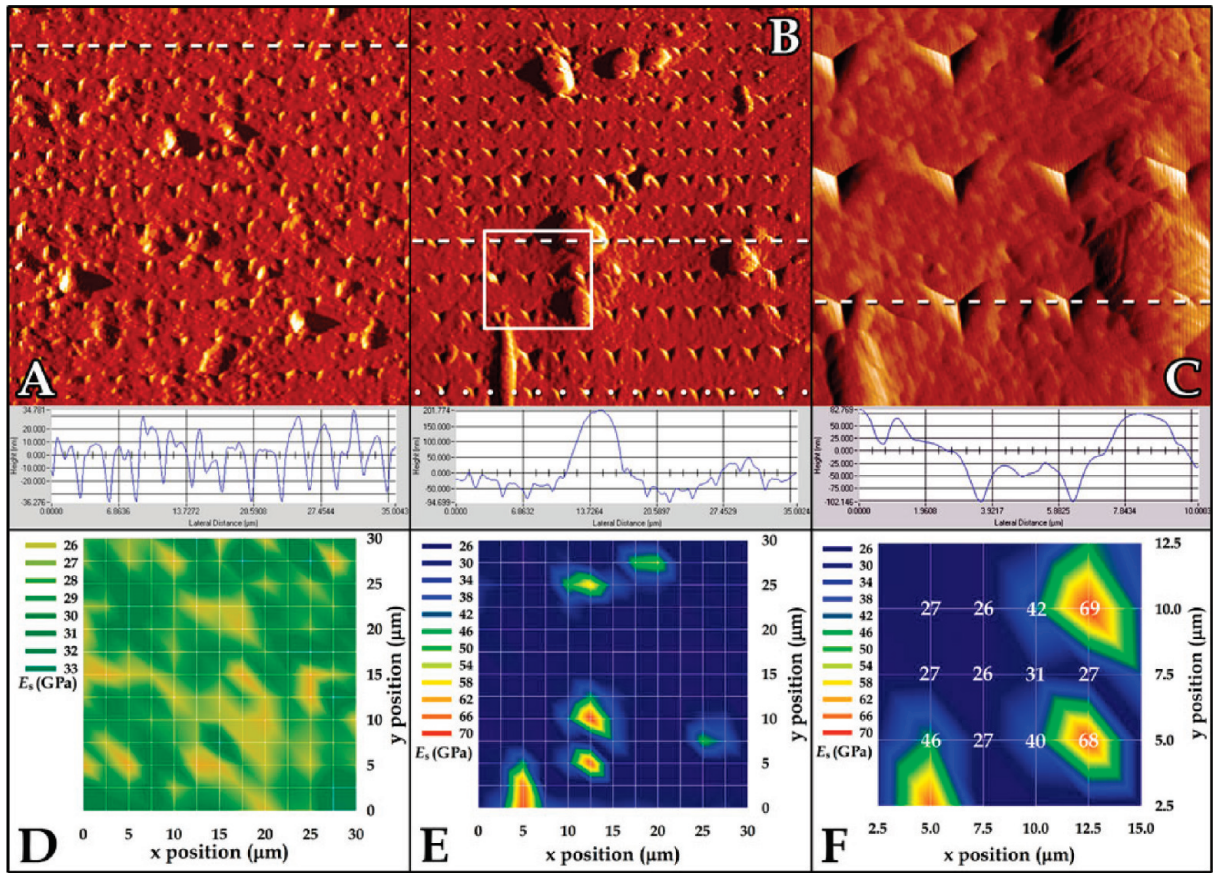

FIGURE 6. AFM images of the arrays of indents on the surfaces of pure CPC (A) and CPC−15%HX biocomposite (B) after NI probing with a peak load of 1 mN (size: 35 × 35 μm). The indicated square area in B is shown enlarged in C (size: 10 × 10 μm). Dashed white lines indicate the set of indents for which the cross-section height profiles are shown in the bottom of the AFM images. Nanoindentation elastic modulus maps (D, E, and F) correspond to the images shown in (A, B, and C). The numbers in F indicate calculated E_s values. The dotted line in B indicates the set of indents for which E_s data points vs position plot are provided as the inset in Figure 7.

in size and depth, as seen from the AFM height profile. The corresponding E_s map (Figure 6D) demonstrates only small variations in the property within the probed region of the cement. The average elastic modulus and hardness of pure CPC are 28.5 ± 2 GPa and 1.2 ± 0.2 GPa, respectively.

The AFM image depicted in Figure 6B shows the array of indents set on the surface of the CPC−15% HX biocomposite. In this AFM image, several spontaneously spatially allocated hydroxyapatite crystals are observed. This indicates that reinforced CPCs do not develop anisotropy of their mechanical properties through orientation of the fibrous/platelet reinforcements. The array is more clearly seen in Figure 6C, which is the the indicated zoomed-in rectangular area in Figure 6B. The indents can be assigned to three different regions: cement, cement−HA crystal vicinity, and HA crystal. This results in a graduation of the mechanical properties within biocomposite, as is evident from the corresponding E_s maps (Figure 6E and F) and the respective elastic modulus vs frequency of appearance plot (Figure 7). As expected, the cement matrix is more compliant and softer than the reinforced phase; in particular, the average elastic moduli and hardness values were calculated to be about 29.7 ± 3.4 GPa and 1.2 ± 0.3 GPa for the cement matrix and 66 ± 7 GPa and 5.7 ± 0.8 GPa for the HA single crystals, respectively. This is further reflected in the larger indent impression on the cement compared to HA particles

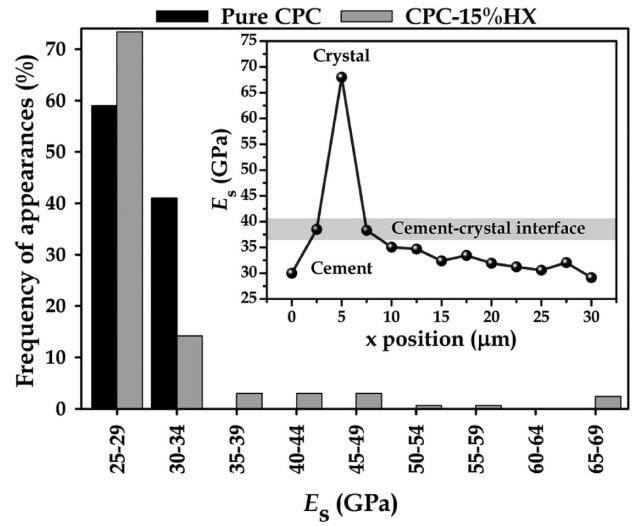

FIGURE 7. Frequency of appearances vs elastic modulus plot for the CPC−15%HX biocomposite. The inset is E_s data points as a function of the distance to the HA particle, plotted for the set of indents indicated by the dotted line in Figure 6B. The solid line connects data points for visual clarity.

(Figure 6B and C). The elucidated vicinity region was further investigated by plotting E_s as a function of the distance to the HA crystal (Figure 7, inset). In the typical example presented, one can clearly observe the gradient of the mechanical properties in the biocomposite going from the

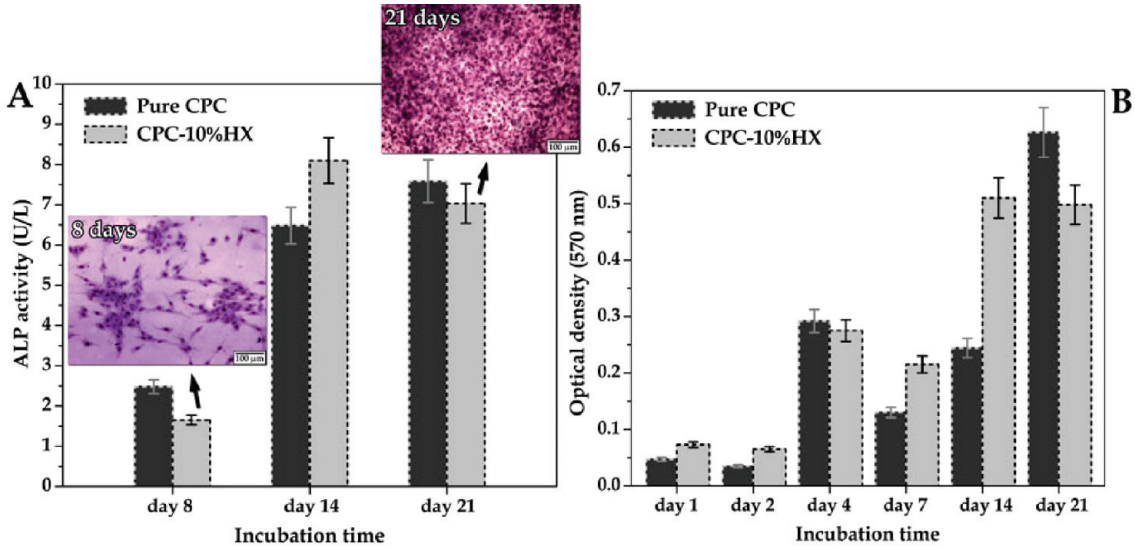

FIGURE 8. Bar graphs of measured ALP (A) and MTT (B) enzyme activities of MC3T3-E1 osteoblast cells cultured on pure CPC and CPC−15%HX biocomposite specimens as a function of time. The insets in A are representative light microscopy images from the Giemsa stained biocomposite surface after 8 (left) and 21 (right) days of cell culture experiments.

HA crystals to the region further away from it. In the current case, the cement−crystal interface is characterized by an elastic modulus of about 38 GPa (Figure 7, inset).

Whereas the mechanical responses from the cement matrix and from stiff HA crystals are expected, the formation of a matrix−filler interface which is stiffer than the cement matrix is somewhat surprising due to the lack of chemical interaction between them. The origin of the interface stiffness is currently not clear. It is well-known that during NI the elastic response of the composite material is due to the long range of the elastic field generated by the indentation load. Therefore, it is possible that the presence of a stiff particle inside the matrix at distances as far as 20 times the indentation depth could affect the measured elastic modulus of the matrix without physically modifying the matrix. This occurs in the same way in a soft film on a hard substrate (26), where elastic moduli higher than the modulus of the film are obtained for a penetration of about 5% of the film thickness. However, according to our NI displacement profiles (not shown), there is a reasonable deformation of the cement matrix under a constant applied load, commonly known as creep. This indicates poor structural regularity of the CPC solid, which leads to a number of slip systems. The porosity of the cement is a major factor that contributes to the slipping (19). Overall, the phenomenon of creep provides a good remedy to the contradictory issue encountered in a soft film/hard substrate system. Hence, it is realistic to expect that the detected cement−crystal interface is not an artifact of the measurements but rather associated with the intrinsic properties of the biocomposite. One possible explanation of such an interface is an inherent elastic modulus gradation of the cement matrix on the cement−crystal interface. For instance, it could be the result of more intensive interlocking CPC nanocrystallites reflected in their closer packaging in the HA crystals vicinity due to a surface-induced crystallization phenomena.

Calcium phosphate cements and hydroxyapatite are both biocompatible; nevertheless, to evaluate whether the HA filler affects the cytotoxicity of the resulting biocomposites, we compared the *in vitro* behavior of the pure CPC and reinforced CPC-15%HX by means of cell culture experiments. The osteoblastic cells' differentiation and proliferation were deduced from the ALP and MTT assays (Figure 8). The cytocompatibilities of the two tested samples are quite alike. Both cement and biocomposite promote cell growth and viability, as evidenced by the observation of the proliferation and differentiation of MC3T3-E1 preosteoblasts toward a mature phenotype over the monitored period of 21 days. The results also show that the presence of the filler HA particles in the cement stimulates preosteoblast differentiation in the early stage of incubation (ALP on days 7−14), while the proliferation of the system becomes steady already in the third week of the experiment (MTT on day 21). Likewise, light microscopic analysis of the Giemsa stained CPC−15%HX at day 8 revealed islands of spindle-shaped preosteoblasts, which seem to be well-adhered to the biocomposite surface (Figure 8A, left insert). Total cell population was significantly enhanced over a period of 21 days. The preosteoblasts are intensively proliferated, resulting in a superior and a sustained covering of the whole exposed CPC−15%HX surface (Figure 8A, right insert). To the first approximation, the results from the cell culture experiment highlight that synthesized biomaterials are cytocompatible and markedly progressive to osteoblastic maturation state.

DISCUSSION

The properties of a composite material strongly depend upon the size, shape, concentration, orientation, and mechanical properties of the filler, and upon the matrix−filler interface as well (27). In the current investigation, the influence of the amount of filler and its particle morphology on the structure and mechanical properties of the biocom-

posites was addressed. Consequently, composite biomaterials having advanced cement (19) as a matrix (compliant cf. filler, E_s ~29.7 GPa) and HA crystals with plate-, needle-, hexagonal prism-, or fine-plate-like shapes (20) as the reinforcement phase (stiffer, E_s ~66 GPa) were prepared. Detailed experimental studies revealed that derived biocomposites are composed of phase-pure hydroxyapatite already after 7 h of the setting reaction.

The observed compression strength results indicate that reinforcement plays an important role in the mechanical performance of the biomaterials. Since CPC is a brittle material, its strength is determined by the largest present cracks, which start to grow once the critical stress is reached (28). If a stronger filler is present in the CPC matrix, it prevents crack propagation by different toughening mechanisms, e.g., fiber pull-out, crack deflection, etc. (27) Electron microscopy observations lead to the conclusion that the reinforced cements are composite materials formed by cement nanoparticles and submicrometer-/micrometer-sized HA crystals intimately associated on the nanometer scale. This strong attachment of the cement to the HA filler crystals most likely contributes to the improved mechanical performance of the as-prepared biocomposites. It is known that the performance of many fiber-containing composite materials is very sensitive to the mechanical properties of the interface region; i.e., interfacial decohesion leads to a reduction in stiffness (29). Moreover, de-adhesion of the matrix−fiber interface is one of the toughening mechanisms that contributes to the increase of fracture toughness of composite materials (27). Hence, the observed stiff interface is a beneficial effect likely causing enhanced consumption of energy for de-adhesion. This may lead to an increase in the fracture toughness parameter of the biocomposite, although in the current study, we did not analyze the mechanism quantitatively. Therefore, additional analyses including fracture toughness and tensile strength are currently underway to rule out the influence of a stiff cement−filler interface on the mechanical properties of the biocomposites.

In addition, the existence of a stiff cement−HA crystal interface (probably due to a more intensive interlocking of CPC nanocrystallites in the proximity of HA crystals) was elucidated by means of nanoindentation. This implies that neutralizing crack propagation in the reinforced cements under mechanical load is enhanced, leading to greater compression strength (16).

It is generally accepted that stiff plate-like inclusions are the most effective in stiffening isotropic composite materials, followed by fibrous-shaped morphologies, with the least effective geometry being spherical (16, 27, 30). In this study, it appears that plate-like particles, having a straight form, are not so effective as reinforcement phases (CPC−10 % PT). A similar low strengthening effect was observed for the CPC−10 % ND composite reinforced with straight needle-like HA particles. In contrast, the CS value obtained for the cement reinforced with hexagonal prism-like particles is considerably higher. This indicates that, for the fillers exhibiting particle sizes on the micrometer scale (Table 1) and similar structural properties (20), the "three-dimensional" shape of the crystals is a more determinant factor of the final mechanical properties. Such a complex shape raises the possibility for enhanced anchoring effects, resulting in better strength performance of the biocomposite.

Nevertheless, the best compression strength performance was achieved by reinforcement of the cement with the fine-plate HA crystals. This modification leads to an enhancement of the CS from 25 MPa for pure CPC to 37 MPa for reinforced CPC, an increase of ~50 %. Such a significant enhancement is most likely related to the synergetic effect of the complementary crystal morphologies of this hydrothermally derived product (20). Furthermore, in contrast to three other micrometer-sized HA fillers, fine-plate HA crystals demonstrate considerably smaller sizes in the submicrometer regime (Table 1). Smaller particles are typically characterized by high specific surface area, providing enhanced attachment and a correspondingly better crack stopping response due to the higher energy consumption for separation. Finally, the use of small particles with complementary shapes may optimize interparticle spacing within a biocomposite batch, observed as an increased overall homogeneity. Hence, CPC−10 % FP is the strongest among the other as-prepared biocomposites.

The biocomposite reinforcement is not only affected by particle shape and size but also controlled by the content of the filler particles. The compression strength showed a volcano-like dependence, having maxima at ~33 MPa and ~37 MPa for the reinforcement by HA crystals with hexagonal-prism- (CPC-15 % HX) and fine-plate-like (CPC-10 % FP) morphologies, respectively. This finding suggests that the strength of the biocomposites at some point starts to be determined by the concentration of the reinforcement phase and not by the inclusion's shape and size, consistent with reported literature (31). It is known that strength is dependent on the intrinsic flaws in the composites, such as pores and reinforced phase aggregates. Therefore, it seems that biocomposites with a high filler content will have high probability and an increased number of strength-determining flaws, leading to a reduced strengthening.

Compared to human bones, the elastic modulus E_s (29.7 GPa) of the cement matrix is slightly higher than that observed for human trabecular bone (15.0−19.4 GPa) (32) and very closed to the range for human cortical bone (20.0−25.8 GPa) (33). The hardness of the cement (1.2 GPa) is higher than observed in human trabecular bone (0.52−0.62 GPa) and is also slightly higher than in human cortical bone (0.62−0.74 GPa) (32). It can be concluded that the as-prepared biocomposites compare closely with human bone in terms of elasticity as well as plasticity. Good biomechanical compatibility requires the elastic moduli of biocomposites and human bone to be closely matched, thus avoiding stress shielding of nearby bone from mechanical forces and the subsequent bone absorption observed when implant materials with a higher elastic modulus than bone are employed as a bone graft.

It is noteworthy that the synthesized biocomposites have significant clinical relevance, as is revealed in the course of the cell culture experiments. This material system is proliferative and differentiative from the preosteoblastic cell line MC3T3-E1, wherein the HA filler is capable of accelerating the overall cell differentiation. This result indicates that produced composites are noncytotoxic and appropriately mimicking aspects of osteoblastic cell growth.

CONCLUSIONS

The mechanical properties of advanced cement were enhanced *via* reinforcement by hydroxyapatite crystals with various particle morphologies. It is shown that the strength performance of these novel reinforced biocomposites is determined by the size, shape, and quantity of the reinforcement phase. The measured mechanical properties of the optimized biocomposites were shown to be very similar to those seen in human bone. This is of great consequence to their potential application in bone repair and substitution, as the biomechanical aspects of calcium phosphate cement biocomposites play a large role in their cytocompatibility and the scope of their application. Fine details about the variations in the micromechanical properties of biocomposites have been demonstrated by means of nanoindentation with its unique spatial resolution.

Acknowledgment. The authors thank Dr. T. Taniguchi for assistance with TEM work; C. Pilz-Allen for help with the cells experiment; and Dr. H. S. Gupta, Dr. A. V. Olenev, and T. P. B. Cotter for helpful discussions. This work was partially supported by the Spanish Ministry of Education and Science (MAT2002-03857) and the European Union Marie Curie EST Fellowship on Biomimetic Systems (MEST-CT-2004-504465).

REFERENCES AND NOTES

(1) LeGeros, R. Z.; Chohayeb, A.; Shulman, A. *J. Dent. Res.* **1982**, *61*, 343.
(2) Brown, W. E.; Chow, L. C. *J. Dent. Res.* **1983**, *62*, 672.
(3) Schmit, J. P.; Hollinger, J. O.; Milan, S. B. *J. Oral Maxillofac. Surg.* **1999**, *57*, 1122–1126.
(4) Larsson, S.; Bauer, T. W. *Clin. Orthop. Relat. Res.* **2002**, *395*, 23–32.
(5) Ginebra, M. P.; Traykova, T.; Planell, J. A. *J. Contr. Release* **2006**, *113*, 102–110.
(6) Bohner, M. *J. Mater. Chem.* **2007**, *17*, 3980–3986.
(7) Dorozhkin, S. V. *J. Mater. Sci.* **2008**, *43*, 3028–3057.
(8) Behiri, J. C.; Bonfield, W. *J. Biomech.* **1984**, *17*, 25–34.
(9) Hench, L. L. *J. Am. Ceram. Soc.* **1991**, *74*, 1487–1510.
(10) Dorner-Reisel, A.; Müller, E.; Tomandl, G. *Adv. Eng. Mater.* **2004**, *6*, 572–577.
(11) Burguera, E. F.; Xu, H. H. K.; Takagi, S.; Chow, L. C. *J. Biomed. Mater. Res., Part A* **2005**, *75A*, 966–975.
(12) Xu, H. H. K.; Simon, C. G. *J. Biomed. Mater. Res., Part A* **2004**, *69A*, 267–278.
(13) Park, K.; Sundaresan, S.; Vasilos, T.; Sung, C. *J. Mater. Res.* **1994**, *9*, 2476–2479.
(14) Kumar, R.; Prakash, K. H.; Cheang, P.; Khor, K. A. *Acta Mater.* **2005**, *53*, 2327–2335.
(15) Knepper, M.; Milthorpe, B. K.; Moricca, S. *J. Mater. Sci. Mater. Med.* **1998**, *9*, 589–596.
(16) Müller, F. A.; Gbureck, U.; Kasuga, T.; Mizutani, Y.; Barralet, J. E.; Lohbauer, U. *J. Am. Ceram. Soc.* **2007**, *90*, 3694–3697.
(17) Suchanek, W.; Yoshimura, M. *J. Mater. Res.* **1998**, *13*, 94–117.
(18) Kasuga, T.; Ota, Y.; Tsuji, K.; Abe, Y. *J. Am. Ceram. Soc.* **1996**, *79*, 1821–1824.
(19) Neira, I. S.; Kolen'ko, Yu. V.; Lebedev, O. I.; Van Tendeloo, G.; Gupta, H. S.; Matsushita, N.; Yoshimura, M.; Guitián, F. *Mater. Sci. Eng., C* **2009**, *29*, 2124–2132.
(20) Neira, I. S.; Kolen'ko, Yu. V.; Lebedev, O. I.; Van Tendeloo, G.; Gupta, H. S.; Guitián, F.; Yoshimura, M. *Cryst. Growth. Des.* **2009**, *9*, 466–474.
(21) Brown, W. E.; Chow, L. C. Dental restorative cement pastes. U.S. Patent No. 4518430, 1985.
(22) Oliver, W. C.; Pharr, G. M. *J. Mater. Res.* **1992**, *7*, 1564–1583.
(23) Turner, C. H.; Burr, D. B. In *Bone mechanics handbook*, 2nd ed.; Cowin, S. C., Ed.; CPC Press: Boca Raton, FL, 2001; pp 7—20.
(24) Grenoble, D. E.; Katz, J. L.; Dunn, K. L.; Gilmore, R. S.; Murty, K. L. *J. Biomed. Mater. Res.* **1972**, *6*, 221–223.
(25) Manjubala, I.; Woesz, A.; Pilz, C.; Rumpler, M.; Fratzl-Zelman, N.; Roschger, P.; Stampfl, J.; Fratzl, P. *J. Mater. Sci. Mater. Med.* **2005**, *16*, 1111–1119.
(26) Bhattacharya, A. K.; Nix, W. D. *Int. J. Solids Struct.* **1988**, *24*, 1287–1298.
(27) Lakes, R. S. In *Biomaterials: Principles and applications*; Park, J. B., Bronzino, J. D., Eds.; CRC Press: Boca Raton, FL, 2003; pp 79—93.
(28) Weibull, W. *J. Appl. Mech. Trans. ASME* **1951**, *18*, 293–297.
(29) Ben Cheokh Larbi, A.; Sai, K.; Sidhom, H.; Baptiste, D. *J. Mater. Eng. Perform.* **2006**, *15*, 575–580.
(30) Roeder, R. K.; Sproul, M. M.; Turner, C. H. *J. Biomed. Mater. Res., Part A* **2003**, *67A*, 801–812.
(31) Xu, H. H. K.; Quinn, J. B.; Smith, D. T.; Giuseppetti, A. A.; Eichmiller, F. C. *Dent. Mater.* **2003**, *19*, 359–367.
(32) Rho, J.-Y.; Roy, M. E.; Tsui, T. Y.; Pharr, G. M. *J. Biomed. Mater. Res., Part A* **1999**, *45*, 48–54.
(33) Guo, X. E. In *Bone mechanics handbook*, 2nd ed.; Cowin, S. C., Ed.; CPC Press: Boca Raton, FL, 2001; pp 9—10.

AM100710B